THE SIMULATION OF TRUCK TIRE ROLLING NOISE

C. Hoever[1] and W. Kropp[2]

Division of Applied Acoustics
Chalmers University of Technology, 41296 Gothenburg, Sweden

The road transportation sector places a severe burden on large parts of the population in the form of road traffic noise. A main contributor to this is the rolling noise generated by the tires of trucks and other heavy vehicles. Advanced simulation tools are not only needed for a better physical understanding of rolling noise generation, but also for the design of quieter tires and road surfaces. So far the development of suitable simulation tools for the prediction of rolling noise has mostly been focussed on car tires. Whether results are applicable to truck tires as well remains unclear. In this study an advanced tool which previously has been successfully used for the simulation of car tire rolling noise is extended and applied to a 315/80 R22.5 truck tire. The sound radiation for steady-state rolling on different road surfaces is calculated and compared to measurements. Very good agreement between simulations and measurements is achieved for the total A-weighted sound pressure level. The agreement between measured and simulated third-octave band spectra is generally good. Finally, the number of different road surface texture scans which are available for a particular road is identified as an important parameter for the quality of the simulations.

1 INTRODUCTION

The road transportation sector places a severe burden on large parts of the population in the form of traffic noise. Possible noise related health issues include an increased risk for cardiovascular diseases, cognitive impairment in children, sleep disturbance, tinnitus and annoyance. As a consequence it is estimated that more than one million healthy life years are annually lost alone in Western Europe [1]. The majority of the traffic-related noise originates from road traffic [1].

In most societies a reduction of road traffic is not in sight. Accordingly, one of the few ways of reducing the impact of road traffic noise is by reducing the sound radiation from the individual vehicle. In the majority of cases these measures are aimed at reducing the noise emission of passenger cars. However, trucks and other heavy vehicles contribute up to 10 % to the overall road mileage travelled [2], and their maximum pass-by levels are about 4 dB to 7 dB higher than those of cars [3]. Accordingly, noise reduction measures for heavy vehicles cannot be neglected.

[1]email: carsten.hoever@chalmers.se
[2]email: wolfgang.kropp@chalmers.se

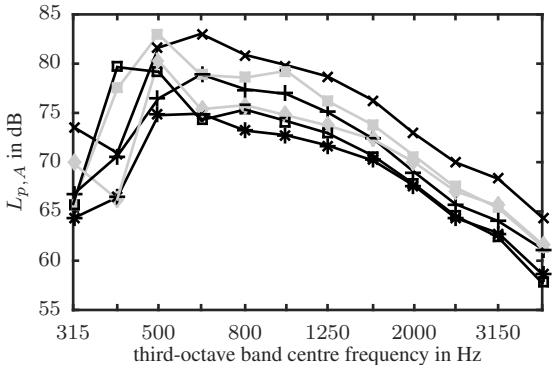

Figure 1: Example of typical truck tire third-octave band rolling noise spectra: close-proximity measurements for two different 315/80 R22.5 tires on two different road surfaces at speeds of $50\,\mathrm{km/h}$ (+/×/∗/□) and $60\,\mathrm{km/h}$ (♦/■). Average of nine microphones equally distributed over a half-circle around the tire at $1\,\mathrm{m}$ from the centre of the contact patch and a height of $0.25\,\mathrm{m}$.

Road traffic noise can be separated into a vehicle's power train noise, rolling noise and aerodynamic noise. At the most typical driving speeds of $30\,\mathrm{km/h}$ to $100\,\mathrm{km/h}$ rolling noise is the dominating noise source, not only for passenger cars but also for trucks [4]. Power train noise dominates at lower and aerodynamic noise at higher speeds. In sum, a substantial part of road traffic noise can be related to truck tires. While this has been recognized by legislative policy makers [5, 6], surprisingly few research has been conducted on truck tire acoustics.

A rolling tire is a complex dynamic system. The tire/road interaction leads to time-varying changes of the tire geometry which ultimately result in sound generation. Several physical mechanisms contribute to rolling noise. It is believed that mainly tire vibrations are responsible for low- and mid-frequency rolling noise up to about $1.25\,\mathrm{kHz}$, whereas aerodynamical mechanisms ("air pumping") dominate above [4]. At typical driving speeds, rolling noise spectra for trucks have their maxima in the frequency region of $500\,\mathrm{Hz}$ to $1\,\mathrm{kHz}$, see Fig. 1. Because of this it is useful to focus on the tire vibrations as a sound source.

The number of radiation models for tire/road noise which are described in open literature is quite small. This does not come as a surprise, as the calculation of sound radiation is an intricate task which requires to develop reliable contact and tire models.

One of the earliest examples of tire sound radiation calculations was by Keltie [7]. He modeled a truck tire as an infinite circular cylindrical shell with a prescribed velocity field, for which sound radiation could be calculated analytically. Ground reflection and the horn effect could not be included because of the omission of the road. A two-dimensional model which accounts for these two effects was presented in [8]. Multipoles were used to model the combined contribution from the tire and the reflection at the road surface. The model was later extended to account for ground impedance effects [9]. In [10] tire/road noise for a three-dimensional patterned tire rolling over a rough road was modeled using a bending plate model in conjunction with a convolution based contact model, and a modified Rayleigh integral approach for radiation. In [11] the same radiation model was used to model the horn effect.

Numerical methods such as finite element modeling (FEM) or boundary element modeling (BEM) have also been used to calculate tire radiation. Using a combined FEM/BEM approach for example, the noise radiation from the tire/wheel assembly was for example modeled in [12]. Because of numerical constraints the road was not included in the model and the frequency range was limited up to $350\,\mathrm{Hz}$. Brick introduced a half-space BEM approach which was used investigate the horn effect [13]. Subsequently, this approach was used together with a waveguide finite element model (WFEM) of the tire and a non-linear time-domain based contact algorithm to calculate the rolling noise of a car tire [14]. Graham [15] combined the mirror

source approach with BEM to investigate the horn effect.

FEM was used to calculate the sound radiation from a truck tire rolling on two different surfaces by Brinkmeier et al. [16], however, results were not compared to measurements.

Apart from the work of Keltie and Brinkmeier et al., none of the studies have been concerned with truck tires. After a phase of intensive research on truck tire vibrations and sound radiation in the United States in the 1970s and early 1980s, e.g. [7, 17–19], research on truck tire acoustics has been rather limited, particularly with respect to sound radiation simulations. While some studies on the low frequency truck tire vibrations have been performed, e.g. [20, 21], acoustically relevant frequency regions were only considered in [22], where an orthotropic plate model was used to simulate truck tire responses up to $4\,\mathrm{kHz}$. Due to the simplicity of the model, results for transfer mobilities were not satisfying.

The lack of dedicated studies on truck tire acoustics is a shortcoming. There is no evidence that findings from studies on car tires are directly applicable to truck tires as well, as there are some major differences between car and truck tires. Besides the obvious dimensional differences several other points also distinguish truck tires from car tires: (i) a higher inflation pressure of up to $900\,\mathrm{kPa}$, (ii) a proportionally thicker tread layer, (iii) the use of steel cords for the ply reinforcement, and (iv) a larger number of steel cord layers in the belt region. As a first consequence the truck tire is considerably stiffer than a car tire.

The present study is based on an extended version of the approach which has successfully been used to calculate exterior car tire rolling noise in [14]. It uses a WFE model of the truck tire, a three-dimensional convolution-based non-linear contact algorithm, and half-space BEM. Exterior tire/road noise is calculated for a 315/80 R22.5 truck tire rolling on a stone mastic asphalt SMA 0/8S , and a low noise asphalt surface LOA 5D. Results are then compared to measurements.

The paper is organized as follows. In Section 2 the tire, contact, and radiation models are presented. Section 3 describes the setup of the measurement and simulations, and analyzes results. In Section 4 some concluding remarks and an outlook for further work are given.

2 THE TIRE/ROAD NOISE MODEL

2.1 Tire modeling

The waveguide finite element approach used for modeling the structural response of the truck tire is in large parts identical to the one applied to car tires in [14, 23]. Therefore, only a very brief overview of WFEM will be given here.

A waveguide is a system with constant geometrical and material properties along one dimension. For a tire, this is the circumference along which the motion can be described by waves fulfilling a periodicity condition $\mathbf{u}(\theta) = \mathbf{u}(\theta \pm 2\pi)$, where $\mathbf{u}$ is the tire displacement and θ the circumferential angle, see Fig. 2b. The waveguide property is used in conjunction with conventional two-dimensional finite element modeling of the waveguide cross-section, see Fig. 2a. Accordingly, the displacement vector $\mathbf{u} = [u_r\ u_x\ u_\theta]^T$ (with $(\bullet)^T$ denoting vector transpose) at a point (r, x, θ) can be split into a cross-sectional component and a circumferential one:

$$u_i(r, x, \theta, t) = \mathbf{N}(r, x)\, \mathbf{v_i}(\theta, t)\,, \qquad i = r, x, \theta\,. \tag{1}$$

$\mathbf{N}$ are the cross-sectional FE shape functions while the degrees-of-freedom at the nodes are given by $\mathbf{v_i}$. Eq. (1) is the basis for the derivation of the WFE tire model, which is described in detail in [24].

Contrary to the implementation for the car tire in [14, 23], solid elements and not shell elements are used for modeling most parts of the tire, see Fig. 2a. This is motivated by a better representation of the thicker truck tire geometry using solid elements. Moreover, there is a reduced need to determine material parameters for elements encompassing several material

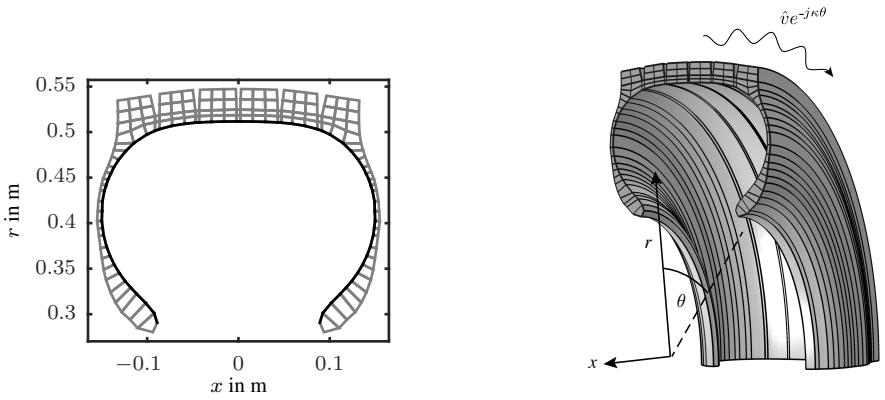

Figure 2: The 315/80 R22.5 tire as a curved waveguide: (a) for the cross-section in the (x, r)-plane an FE approximation (shell elements black, solid elements gray) is used, while (b) in circumferential direction θ wave propagation is assumed. Waves traveling in negative θ direction have to be considered as well, but are not shown here.

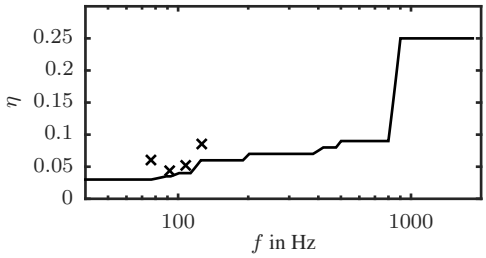

Figure 3: Loss factors for proportional damping for the 315/80 R22.5 tire. Results from half-power bandwidth measurements marked by $\times$.

groups. In total 126 anisotropic quadrilateral Lagrange type elements with nine nodes are used to model the tire cross-section. In addition, 65 anisotropic, 3-node doubly-curved deep shell elements accounting for rotational inertia, shearing across the thickness and pre-tension model the ply. In the circumferential direction the tire is divided into 912 segments.

The air cavity is not explicitly modeled; the inflation pressure of $670\,\mathrm{kPa}$ is included by means of the resulting pre-tension. Rolling is calculated for a tire without a wheel, instead tire motion is blocked at the bead. The tire's read pattern is limited to the pronounced circumferential grooves shown in Fig. 2a.

Geometry and bulk material data for $20\,°\mathrm{C}$ were provided by the manufacturer. Based on data on dynamic viscoelastic material behavior, Young's moduli for rubber materials are assumed to be frequency dependent below $200\,\mathrm{Hz}$. For higher frequencies constant values are used. The procedures outlined in [25, Chap. 5] are used to determine the element pre-tension and the material parameters for elements containing more than one material group, for example in the belt or bead regions. The frequency-dependent loss factor for proportional damping is shown in Fig. 3. It is based on half-power bandwidth estimations and further optimization of simulated mobilities towards measurements.

Due to material changes during tire curing and uncertainties in the material parameter condensation process, a manual adjustment of the radial extensional and lateral shear stiffness terms is necessary in the belt region. The shell pre-tension is furthermore increased by $30\,\%$ in lateral direction and reduced by $20\,\%$ in circumferential direction. With these values good agreement between measured and simulated forced responses is obtained, as can be seen Fig. 4.

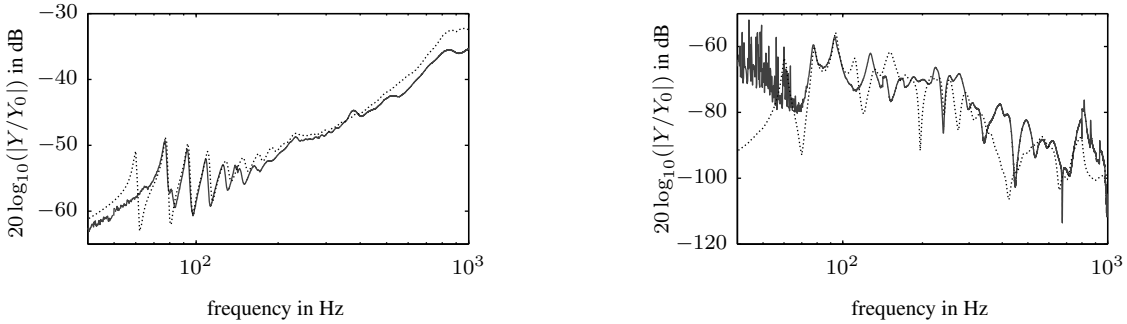

(a) magnitude input mobility

(b) response at outer tread band, $120°$ ($1.15\,\mathrm{m}$) from excitation

Figure 4: Comparison of radial input and transfer mobilities Y from measurement (—) and simulations ($\cdots$). Additional first resonance in simulations due to differences in boundary conditions between measurements and simulations. $Y_0 = 1\,\mathrm{N/(ms)}$.

The forced response measurement procedure is identical to the one for a car tire described in [25]. In the measurements, no clamped rim boundary condition could be achieved for the truck tire. Instead a freely-suspended tire was used. The consequence is that the peak at $60\,\mathrm{Hz}$ (i.e. the translational semi-rigid body mode [25]) is only visible in the simulations.

In Fig. 4a excellent agreement between measured and simulated radial input mobilities is achieved between $70\,\mathrm{Hz}$ and $150\,\mathrm{Hz}$. Between $150\,\mathrm{Hz}$ and $200\,\mathrm{Hz}$ there is a slight overestimation of frequencies and amplitudes in the simulations. Above $400\,\mathrm{Hz}$ the amplitude is again slightly overestimated. In Fig. 4b results for transfer mobilities are shown. There is very good agreement between measured and simulated mobilities at low frequencies. At higher frequencies there are some small frequency and/or amplitude shifts but most of the features of the measured mobilities are captured well by the simulations. Average orders of response magnitude agree very well over the whole frequency region.

2.2 Tire/road interaction

The contact model is based on the convolution approach originally developed for tires by one of the authors [8], and its subsequent enhancements by several authors (e.g. [23, 26]).

The time-dependent position of a point e on the tire surface can be written as

$$Z_e(t) = Z_{T,e}(t) + u_e(t)\,, \tag{2}$$

where $Z_{T,e}(t)$ is the tire contour as shown in Fig. 5. Present and past forces cause a tire vibration $u_e(t)$, given by

$$u_e(t) = \sum_m \int_{-\infty}^{\infty} F_m(\tau)\, g_{m,e}(t-\tau)\, d\tau\,, \tag{3a}$$

where $g_{m,e}$ is the displacement Green's function for a point e due to a force at point m. It is obtained by inverse Fourier transform of input and transfer receptances as given by the WFE tire model. The time discretized version of (3a) for $t_N = N\Delta t$ and all possible contact points $e = 1 \ldots M$ is given as [27]

$$\mathbf{u}(t_N) = \mathbf{G}_0\, \mathbf{F}(t_N) + \mathbf{u}_{\text{old}}(t_N)\,. \tag{4}$$

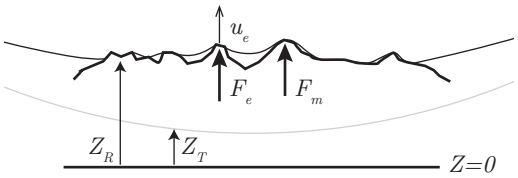

Figure 5: Contact between tire and road. The undeformed tire contour (grey) is given by Z_T and the road roughness profile by Z_R. F_e and F_m are the contact forces acting at points e and m, and u_e is the dynamic response of the structure in point e.

Here, $\mathbf{G}_0$ is a $M \times M$ matrix containing the values of the Green's functions for $t = 0$. The second term in (4) represents past, known values of the contact forces and can be considered a constant at each time step.
From the boundary conditions at the tire/road interface it furthermore follows

$$\mathbf{d}(t_N) = \mathbf{Z_R}(t_N) - \mathbf{Z_T}(t_N) - \mathbf{u}(t_N)\,, \tag{5a}$$
$$F_e(t_N) = k\, d_e(t_N) \cdot \mathcal{H}\{d_e(t_N)\} \tag{5b}$$

where $\mathbf{d}$ contains the distances d_e between tire contour and road surface. The road penetrates into the tire at a contact point e if $d_e > 0$. $\mathcal{H}$ is the Heaviside operator and k the stiffness of a contact spring which is added between tire and road at each point e. These springs account for the influence of the small-scale roughness on the area of contact between the contacting bodies [23].

Equations (4) and (5) formulate a non-linear contact problem which is solved iteratively for every time-step to obtain the contact forces. After Fourier transformation to the frequency domain these are used as excitation for the WFE tire model. The result is the vibrational field of a tire rolling on a road which can be used as input into the radiation model.

2.3 Radiation modeling

A half-space BEM approach [14] is used to model the sound radiation from the tire. In this approach the ground is not explicitly modeled, the reflection from the road surface is instead included via specially derived Green's functions [13].

The spatial resolution of the tire's vibrational field, which serves as the input data for the BEM calculations, is given by the cross-sectional WFEM mesh and the circumferential discretization as used in the contact modeling. To lower the numerical effort the mesh is reduced to 31 elements over the cross section and 151 over the circumference for the BEM calculations. This is sufficient for frequencies up to $2.5\,\mathrm{kHz}$. The mesh is based on the deformed tire shape under static loading to properly account for the horn effect. Finally, rigid wheel covers are added on both tire sides. The resulting mesh is shown in Fig. 6. Twelve CHIEF points are randomly distributed inside the tire to avoid numerical irregularities.

3 ROLLING NOISE SIMULATIONS

3.1 Setup

Simulations are performed for an SMA 0/8S and a LOA 5D surface. Both surfaces are samples from test fields at a dedicated test site in Geilenkirchen, Germany. Surface texture scans were

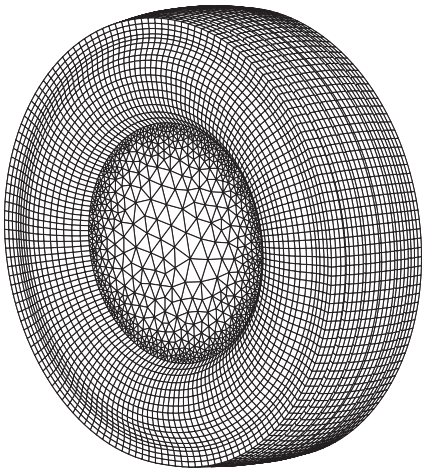

Figure 6: The mesh used for the BEM calculations.

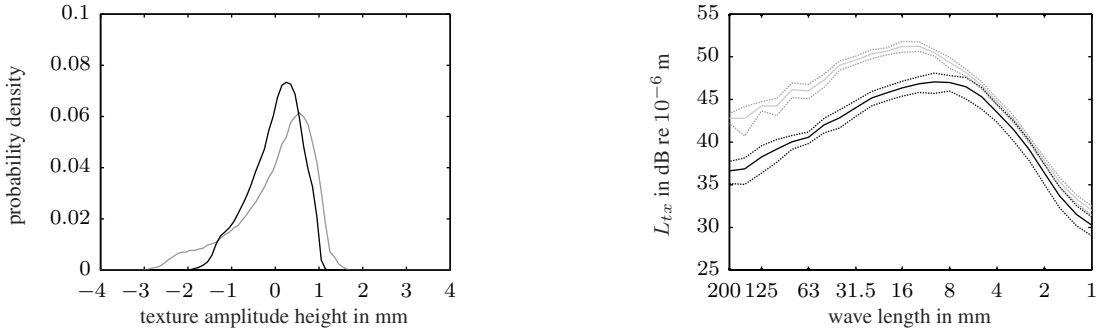

(a) profile amplitude distribution

(b) road surface spectrum

Figure 7: Properties of the SMA 0/8S (gray) and LOA 5D (black) road surfaces: (a) profile amplitude distributions, and (b) third-octave band average (—) and standard deviation ($\cdots$) of the road surface spectra over all lateral tracks and all measurement positions.

performed at six different positions in each test field. For each position scans of ten parallel tracks of length $1.96\,\mathrm{m}$ and a lateral spacing of $0.01\,\mathrm{m}$ are available. The scan resolution in rolling direction is $0.2\,\mathrm{mm}$. For the simulations the roughness profile is resampled to match the resolution of the tire model.

In Fig. 7 the profile amplitude distributions and the average third-octave band surface spectra L_{tx} are given for both surfaces. The SMA 0/8S surface has a broader profile amplitude distribution, see Fig. 7a, and a road surface spectrum which is between $2\,\mathrm{dB}$ (at low wave lengths) to $6\,\mathrm{dB}$ (at large wave lengths) higher, see Fig. 7b. This means the SMA 0/8S is the "rougher" surface. Also shown in Fig. 7b is the standard deviation between the different texture profile scan locations for a particular road surface. For the SMA 0/8S the standard deviation is in the range of $1.0\,\mathrm{dB}$ for all wave lengths, whereas for the LOA 5D it is about $1.0\,\mathrm{dB}$ at long wave lengths and reduces to around $0.5\,\mathrm{dB}$ at shorter wave lengths. The relatively homogenous surface properties over the whole test field for most wave lengths are important with respect to the rolling noise measurements. These utilize larger areas of the test field as the surface scans can encompass.

Tyre/road noise measurements were carried out using a dedicated measurement trailer as described in [28]. Nine microphones were mounted around the tire as shown in Fig. 8. Third-octave bands from $315\,\mathrm{Hz}$ to $5\,\mathrm{kHz}$ were covered in the measurements.

(a) front view (b) top view

Figure 8: Microphone positions for the measurements. Each ● marks one microphone/field point. The microphones are placed at an angular distance of $22.5°$ on a half-circle of radius $1\,\mathrm{m}$ from the tire centre. The height is $0.25\,\mathrm{m}$ over the ground.

For the simulations the same nine points are used to evaluate the sound pressure. Moreover, additional field points are added every two degrees on the half-circle to minimize the influence of possible directivity deviations. Rolling noise is calculated separately for each of the six texture profile measurement positions within a particular road surface test field. The average and the range of the sound pressures are determined and the corresponding sound pressure levels are calculated.

The measurements were conducted with an axle load of $2000\,\mathrm{kg}$ and a driving speed of $60\,\mathrm{km/h}$. The same values are used for the simulations. Rolling is calculated for five full tire revolutions of which the last one is evaluated. Based on the circumferential tire resolution this gives a frequency resolution of roughly $5\,\mathrm{Hz}$ and a maximum frequency of $2210\,\mathrm{Hz}$. For the contact springs values of $k = 1.25 \cdot 10^4\,\mathrm{N{\cdot}m^{-1}}$ and $k = 0.81 \cdot 10^4\,\mathrm{N{\cdot}m^{-1}}$ are used for the SMA 0/8S and LOA 5D surfaces, respectively. These values give the right contact patch size compared to measurements.

3.2 Results

Comparisons between the measured and simulated A-weighted third-octave band rolling noise spectra are shown in Fig. 9. For the SMA 0/8S surface in Fig. 9a the shape of the simulated and the measured spectra is similar. Nearly perfect agreement in sound pressure levels is obtained for the $630\,\mathrm{Hz}$ third-octave band where the maximum of the measured rolling noise spectrum is located. For lower frequencies the simulations overestimate the measured values by $2.6\,\mathrm{dB}$ in the $315\,\mathrm{Hz}$ and $500\,\mathrm{Hz}$ third-octave bands, and by $6.7\,\mathrm{dB}$ in the $400\,\mathrm{Hz}$ band. From $800\,\mathrm{Hz}$ to $1.25\,\mathrm{kHz}$ good agreement is achieved with an underestimation of maximum $1.6\,\mathrm{dB}$ in these frequency bands. For higher frequencies the deviation increases to $3.2\,\mathrm{dB}$ at $2\,\mathrm{kHz}$. The total A-weighted sound pressure level is $85.4\,\mathrm{dB}$ for both the measurement and the simulations. A large part of this excellent agreement can be attributed to the accurate prediction of the peak sound pressure level in the $630\,\mathrm{Hz}$ third-octave band. However, it has to be acknowledged that the overestimation of the measured levels for low frequencies and the underestimation for high frequencies seem to cancel each other out in a beneficial way.

Even better agreement is obtained for the LOA 5D surface in Fig. 9b: between $315\,\mathrm{Hz}$ and $1.25\,\mathrm{kHz}$ the average difference between measured and simulated spectrum is roughly $1.0\,\mathrm{dB}$, with a maximum deviation of $2.0\,\mathrm{dB}$ at $400\,\mathrm{Hz}$. For higher frequencies the differences are more pronounced with an underestimation of the measurement results by $2.5\,\mathrm{dB}$ at $1.6\,\mathrm{kHz}$ and $4.0\,\mathrm{dB}$

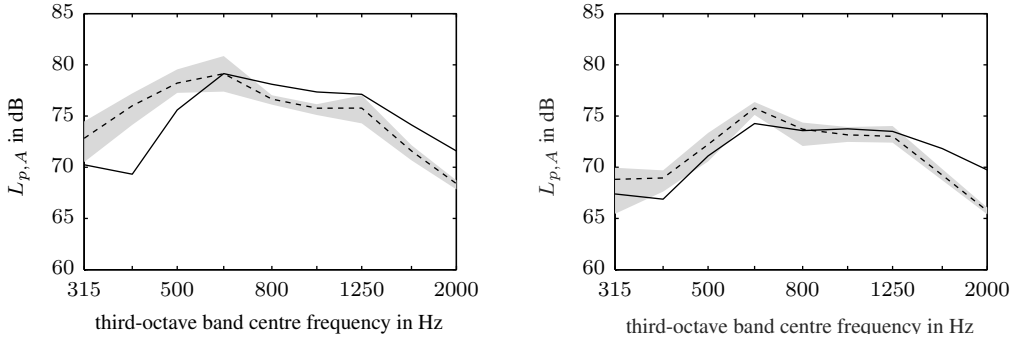

(a) SMA 0/8S (b) LOA 5D

Figure 9: Measured (—) and simulated (– –) third-octave band rolling noise spectra. Simulation based on the average sound pressures for all six measurement positions. Grey shading indicates range of results from individual surface scan positions.

at 2 kHz. The agreement of the overall A-weighted sound pressure level is again excellent with 81.6 dB measured and 81.7 dB simulated.

In Fig. 9 the simulated rolling noise levels are too high for low frequencies, especially for the SMA 0/8S surface in Fig. 9a. It is apparent that this overestimation starts to appear for third-octave bands for which the wave length is in the order of the distance of the microphones/field points to the tire. Accordingly, near field effects are to be expected for these frequencies. It is possible that the near field is not captured in the same way in the measurements and the simulations.

That the simulated sound pressure levels are too low for higher frequencies can be explained by an increasing importance of aerodynamical source mechanisms for rolling noise at frequencies of about 1 kHz [4]. Aerodynamic mechanisms are not accounted for in the simulations and hence a certain underestimation of measured sound pressure levels can be expected at high frequencies.

In Fig. 9 an important observation can be made regarding the range of the simulated sound pressure levels over the different surface scan positions: for the majority of third-octave bands up to 1250 Hz band, the A-weighted range between the highest and lowest calculated level is between 2 dB to 4 dB. This is regardless of the surface. This emphasizes the necessity to base the simulations on road surface scans from several locations in the test field. Otherwise there is a risk of obtaining non-representative results; not only for certain frequency bands but possibly also for the total sound pressure level. For higher frequencies the range reduces to maximum 1.5 dB, indicating that the variations in sound pressure levels are possibly related to the slightly larger texture amplitude variations at longer wave lengths in Fig. 7b.

Some examples of the directivity of the sound radiation are shown in Fig. 10. For the measurements maximum values are always obtained exactly in the front/rear of the tire. This is not the case for the simulations where for both surfaces radiation is highest directly to the side for all third-octave bands apart from the 1.6 kHz one. Fig. 10a gives some insight into why the simulations overestimate the sound pressure levels at lower frequencies: compared to the measurements levels are nearly identical at the front and rear, yet there is too much sidewall radiation. With increasing frequency, see the 630 Hz and 1 kHz results in Figures 10b and 10c, there is better agreement between measurements and simulations for the lateral direction. At the same time there is an increasing tendency of underestimated sound pressures in the front and rear. This might again be related to an increasing importance of aerodynamic sources. Interesting are the results for the 1.6 kHz third-octave band in Fig. 10d. The simulated sound pressure is, with the exception of a small area around 60°, again too low. This could be expected from

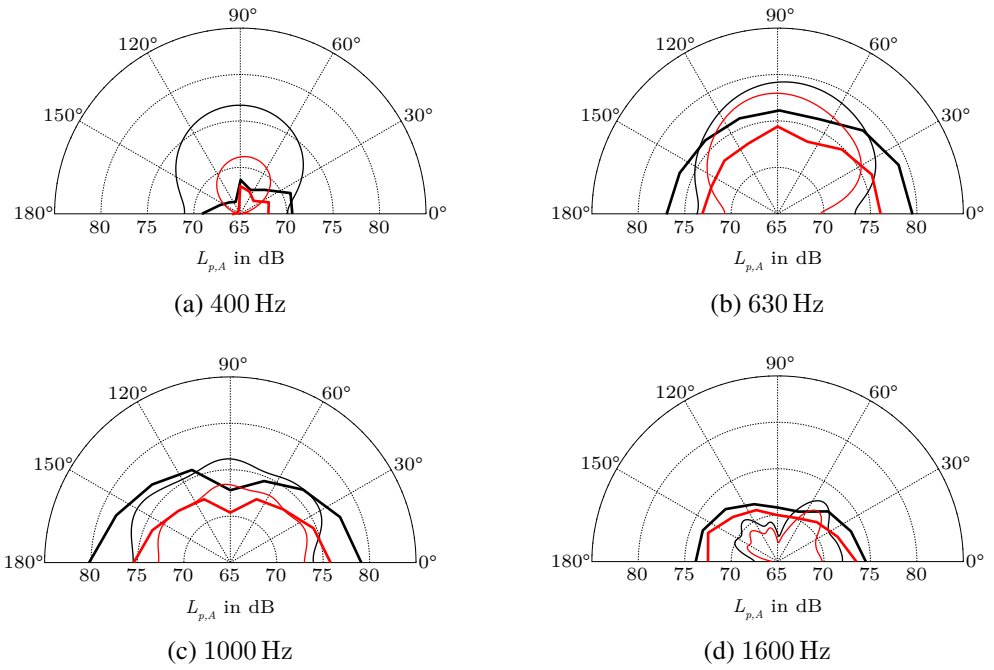

(a) 400 Hz (b) 630 Hz

(c) 1000 Hz (d) 1600 Hz

Figure 10: Directivity for measurements (thick lines) and simulations (thin lines). SMA 0/8S in black, LOA 5D in red. View corresponds to Fig. 8b with the tire rolling to the right.

the rolling noise spectra in Fig. 9. Somewhat surprising is the difference in the general shape between the directivity of the measured and the simulated radiation. The measurements are characterized by an elliptical directivity which favors the front and aft of the tire. The simulations, in contrast, show a directivity pattern with distinct lobes around $60°$ and $120°$, and minima at $90°$ and $180°$. This shows that the relevant sound source in the measurements continues to be small compared to the wave length whereas this is not the case anymore for the simulations. This is another indication for over-proportionally high contribution of sidewall radiation in the simulations.

A slight uncertainty about the measurement results in Fig. 10d remains because the accuracy of the directivity suffers somewhat from the limited number of microphones. Furthermore, it is not clear if and how measurement results are possibly affected by the measurement trailer, for example due to reflections.

Finally, the results shown in Fig. 7 indicated that the SMA 0/8S is a rougher surface than the LOA 5D. This is reflected by the rolling noise spectra results shown in Fig. 9. All individual third-octave band values for the SMA 0/8S are higher than the corresponding levels for the LOA 5D: by around $2.5\,\mathrm{dB}$ at lower frequencies, by around $4.5\,\mathrm{dB}$ between $630\,\mathrm{Hz}$ and $1250\,\mathrm{Hz}$, and by $2.0\,\mathrm{dB}$ at and above $1.6\,\mathrm{kHz}$.

4 CONCLUDING REMARKS AND OUTLOOK

A method for calculating the rolling noise of a truck tire rolling on a real road surface under steady-state conditions has been presented. As an example, the sound radiation from a 315/80 R22.5 tire rolling on two different road surfaces has been calculated and compared to measurements.

Excellent agreement between simulations and measurements has been achieved for the total A-weighted sound pressure level. The dominating third-octave bands in the rolling noise spectrum are also very well predicted, especially for the LOA 5D surface. However, regardless of surface, an overestimation of the measured spectrum can be observed for lower frequencies, and

an underestimation at higher frequencies. The high frequency differences can be explained by not accounting for aerodynamic mechanisms in the simulation tool. Near field effects might by the reasons for the low frequency deviations. Based on a directivity analysis there is also too much radiation from the tire side in the calculations.

The study also reveals that local roughness variations can have a significant influence on the simulated rolling noise spectrum. For some frequency bands several dB difference in calculated rolling noise can be observed depending on where on the surface the profile scan was taken. This means that it is necessary to calculate the average rolling noise for several surface scans of a particular road segment. Otherwise results are possibly not representative and cannot be compared to pass-by or close-proximity measurements.

As a next step the proposed method needs to be further verified different road surfaces. Preferably, this should include far field measurements as well. This will hopefully also help to determine the exact reasons for the observed deviations of the low- and high-frequency spectra and the directivity.

5 ACKNOWLEDGEMENTS

The funding from the project *LeiStra3* (Leiser Straßenverkehr 3), financed by the German Federal Ministry for Economic Affairs and Energy, and the German Federal Ministry of Transport and Digital Infrastructure, is gratefully acknowledged.

REFERENCES

[1] Burden of disease from environmental noise — Quantification of healthy life years lost in Europe. Report, WHO, 2011.

[2] U. Kunert, S. Radke, D. Chlond, and M. Kagerbauer. Auto-Mobilität: Fahrleistungen steigen 2011 weiter. *DIW Wochenbericht*, 47.2012:3–14, 2012.

[3] E. Schreurs, L. Brown, and D. Tomerini. Maximum pass-by noise levels from vehicles in real road traffic streams: Comparison to modeled levels and measurement protocol issues. In *Proceedings of Internoise 2011, Osaka, Japan*, 2011.

[4] U. Sandberg and J.A. Ejsmont. *Tyre/road noise reference book*. Informex, 2002.

[5] EC regulation 1222/2009 on the labelling of tyres with respect to fuel efficiency and other essential parameters. Official Journal L 342, December 2009.

[6] UNECE Reg. 117 - Uniform provisions concerning the approval of tyres with regard to rolling sound emissions and to adhesion on wet surfaces and/or to rolling resistance, 2011.

[7] R.F. Keltie. Analytical model of the truck tire vibration sound mechanism. *J. Acoust. Soc. Am.*, 71(2):359–367, 1982.

[8] W. Kropp. *Ein Modell zur Beschreibung des Rollgeräusches eines unprofilierten Gürtelreifens auf rauher Straßenoberfläche*. Number 166 in Fortschrittberichte VDI, Reihe 11: Schwingungstechnik. VDI Verlag, 1992.

[9] F.-X. Bécot. *Tyre noise over impedance surfaces — Efficient application of the equivalent sources method*. PhD thesis, Chalmers Univ. of Techn. Gothenburg/INSA Lyon, 2003.

[10] D.J. O'Boy and A.P. Dowling. Tyre/road interaction noise — Numerical noise prediction of a patterned tyre on a rough road surface. *J. Sound Vib.*, 323(1-2):270–291, 2009.

[11] R.A.G. Graf. *Tyre-road interaction noise*. PhD thesis, Univ. of Cambridge, 2002.

[12] E.-J. Ni, D.S. Snyder, G.F. Walton, N.E. Mallard, G.E. Barron, J.T. Browell, and B.N. Aljundi. Radiated noise from tire/wheel vibration. *Tire Sci. Technol.*, 25(1):29–42, 1997.

[13] H. Brick. *Application of the Boundary Element Method to combustion noise and half-space problems*. PhD thesis, Chalmers Univ. of Techn., 2009.

[14] W. Kropp, P. Sabiniarz, H. Brick, and T. Beckenbauer. On the sound radiation of a rolling tyre. *J. Sound Vib.*, 331(8):1789–1805, 2012.

[15] W.R. Graham. Influence of tire geometry on the horn effect. In *Proceedings of the Inter-noise 2012, New York City, NY, USA*, 2012.

[16] M. Brinkmeier, U. Nackenhorst, S. Petersen, and O. von Estorff. A finite element approach for the simulation of tire rolling noise. *J. Sound Vib.*, 309(1-2):20–39, 2008.

[17] W.F. Reiter, A.C. Eberhardt, and L.J. Harper. Truck tire vibration/noise. In *NoiseCon73, Washington DC*, pages 202–205, 1973.

[18] A.C. Eberhardt. Truck tire vibration sound. In *InterNoise80, Miami*, pages 281–284.

[19] A.C. Eberhardt. Source identification of the noise from non-stationary truck tire vibration and sound. In *NoiseCon81, Raleigh, USA*, pages 43–48, 1981.

[20] X. Zhang, S. Rakheja, and R. Ganesan. Modal analysis of a truck tyre using FE tyre model. *Heavy Veh. Syst.*, 11(2):133–154, 2004.

[21] A. Miège and A. Popov. Truck tyre modeling for rolling resistance calculations under a dynamic vertical load. *Proc. Inst. Mech. Eng. D J. Automob. Eng.*, 219(4):441–456, 2005.

[22] P.A. Dinkova and W. Kropp. Modeling the vibrational response of truck tyres. In *Proceedings of Euronoise 2006, Tampere, Finland*.

[23] C. Hoever and W. Kropp. A model for investigating the influence of road surface texture and tyre tread pattern on rolling resistance. *J. Sound Vib. (In Press)*, http://dx.doi.org/10.1016/j.jsv.2015.04.009i, 2015.

[24] S. Finnveden and M. Fraggstedt. Waveguide finite elements for curved structures. *J. Sound Vib.*, 312(4–5):644–671, 2008.

[25] C. Hoever. *The influence of modeling parameters on the simulation of car tyre rolling losses and rolling noise*. Licentiate thesis, Chalmers Univ. of Techn., Gothenburg, 2012.

[26] F. Wullens and W. Kropp. A three-dimensional contact model for tyre/road interaction in rolling conditions. *Acta Acust. United Ac.*, 90(4):702–711, 2004.

[27] K. Larsson. *Modelling of dynamic contact — Exemplified on the tyre/road interaction*. PhD thesis, Chalmers Univ. of Techn., Gothenburg, 2002.

[28] W. Schwanen, H.M. van Leeuwen, A.A.A. Peeters, G.J. van Blokland, H.F. Reinink, and W. Kropp. Acoustic optimization tool — RE3: Measurement data Kloosterzande test track. Technical Report M+P.DWW.06.04.8, M+P - consulting engineers, 2007.